Phys Chem Minerals
DOI 10.1007/s00269-014-0710-0

ORIGINAL PAPER

Compressibility of carbonophosphate bradleyite $Na_3Mg(CO_3)(PO_4)$ by X-ray diffraction and Raman spectroscopy

Jing Gao · Weifeng Huang · Xiang Wu · Dawei Fan · Ziyu Wu · Dingguo Xia · Shan Qin

Received: 21 April 2014 / Accepted: 30 August 2014

Abstract Bradleyite $Na_3Mg(CO_3)(PO_4)$ is one typical carbonophosphate, representing dual properties of both carbonates and phosphates. Compressibility of bradleyite has been investigated using synchrotron radiation X-ray diffraction and Raman spectroscopy combined with diamond anvil cells up to 41 GPa at room temperature. Experimental results clearly demonstrate that bradleyite is stable in the investigated pressure conditions. Isothermal pressure–volume relationship has been fitted to the third-order Birch–Murnaghan equation of state with $K_0 = 65.9(9)$ GPa, $K_0' = 3.08(3)$ and $V_0 = 301.4(4)$ Å^3. The crystallographic axes exhibit similar and considerable compressibility up to ~16 GPa, but an increasing anisotropy can be defined thereafter because the *b-axis* becomes more and more rigid. Insight into the behaviors of $[PO_4]^{3-}$ and $[CO_3]^{2-}$ groups have been obtained using Raman spectroscopy, with the symmetrical stretching bands being observed at 970.8 and 1,078.7 cm^{-1}, respectively. Both modes shift to higher frequencies on compression. The pressure coefficient of Raman shifts in C–O is 3.18(2) × 10^{-3} cm^{-1}/GPa, and the value of Grüneisen parameters (γ) is ~0.22. $[PO_4]^{3-}$ groups in bradleyite exhibit a mode hardening, with a slope of 3.54(6) × 10^{-3} cm^{-1}/GPa, γ = ~0.24 below ~16 GPa, and of 2.37(1) × 10^{-3} cm^{-1}/GPa, γ = ~0.16 thereafter. The mode hardening may indicate correlations to the increase in symmetry of the local environment around the $[PO_4]$ tetrahedra. The low γ values are compatible with the rigidness of $[CO_3]^{2-}$ and $[PO_4]^{3-}$ in bradleyite, which have, respectively, been documented in carbonates and phosphates. Our present study may open new perspectives on the Earth carbon and phosphorus cycle, arouse the interest in carbonophosphate minerals, and shed light on other $[CO_3]^{2-}$ and $[PO_4]^{3-}$ coexistent phases.

Keywords Carbonates · Phosphates · Compressibility · Diamond anvil cell

J. Gao · X. Wu (✉) · S. Qin (✉)
Key Laboratory of Orogenic Belts and Crustal Evolution, MOE, School of Earth and Space Sciences, Peking University, Beijing 100871, China
e-mail: xiang.wu@pku.edu.cn

S. Qin
e-mail: sqin@pku.edu.cn

W. Huang · Z. Wu
National Synchrotron Radiation Laboratory, University of Science and Technology of China, Hefei 230029, China

W. Huang · D. Xia
College of Engineering, Peking University, Beijing 100871, China

D. Fan
Laboratory for High Temperature and High Pressure Study of the Earth's Interior, Institute of Geochemistry, Chinese Academy of Sciences, Guiyang 550002, China

Introduction

Carbonates and phosphates have long been considered as, respectively, the main phases of $[CO_3]^{2-}$ or $[PO_4]^{3-}$ groups in the Earth's crust. By subduction of oceanic lithosphere, carbonates and phosphates can be transported into the Earth's mantle, which are of significant implications to the Earth carbon and phosphorus cycle and the mantle evolution. Their high-pressure properties therefore have been extensively investigated, including chemical components, structural stabilities and elastic properties.

Among all the carbonates, magnesite $MgCO_3$ is widely believed as the most likely reservoir for oxidized carbon in the Earth's interior because of its dominant content

Published online: 17 September 2014

(Oganov et al. 2006) and structural stability in the presence of silicates (Biellmann et al. 1993). Although the oxygen fugacity of the transition zone and lower mantle is most likely favorable to diamond or methane etc., an influx of subduction-related carbonate melt would oxidize certain regions to allow the existence of magnesite (Stagno et al. 2011). Since the incorporation of Fe could significantly modify the phase relationships of carbonates (Martin and Hammouda 2011) and stabilize the ternary Ca–Mg–Fe carbonates at moderate pressures (Franzolin et al. 2011), ferromagnesite (Mg, Fe)CO_3 has consequently been proposed and documented to be another main carbon carrier during the subduction down to the deep Earth (Boulard et al. 2012; Lin et al. 2012). Pure dolomite (Ca,Mg)CO_3 has proved to decompose into a denser magnesite + aragonite phase at ~7 GPa (Martinez et al. 1996; Buob et al. 2006), but the minute contamination of Fe could improve its stability up to 17 GPa and stabilize its high-pressure polymorphs to the lower mantle conditions (Mao et al. 2011; Merlini et al. 2012a). It is thus suggested that Fe-doped dolomite should also be a potential host of carbon in the mid-to-deep mantle. However, for calcite $CaCO_3$, which is an unstable carbon-bearing phase with pressure as it converts to calcite-II ($P2_1/c$ and $Z = 4$) at ~1.5 GPa (Merrill and Bassett 1975), then to calcite-III (P-1 $Z = 10$ for IIIa and P-1 $Z = 4$ for IIIb) at ~2.5 GPa (Merlini et al. 2012b) and later to be in the aragonite phase up to 42 GPa (Ono et al. 2005), the substitution of Fe for Ca does not occur with ease because Ca^{2+} (1.00 Å, Shannon 1976) >Fe^{2+} (0.78 Å, Shannon 1976) (Goldsmith et al. 1962). In addition to these dominant carbonates, a number of investigations also focus on rhodochrosite $MnCO_3$, otavite $CdCO_3$ and smithsonite $ZnCO_3$ etc. Rhodochrosite has been evidenced to transform into a new orthorhombic structure at 50 GPa after laser heating (Ono 2007), which is also observed in otavite at ~18 GPa and 1,000 °C (Liu and Lin 1997; Minch et al. 2010), and smithsonite has lately been demonstrated stable up to 50 GPa at room temperature (Gao et al. 2014). These carbonates are not deemed as main roles in the Earth carbon cycle because of their low-content in the mantle.

As the main phosphorus phases, the stability of phosphates are essential to understand the Earth phosphorus cycle; besides, their high-pressure behaviors are also of implications to the mantle evolution because they can incorporate large ion lithophile elements (LILE) (e.g. Sr and Ba) and rare earth elements (REE) (Sugiyama and Tokonami 1987; Zhai et al. 2009) in the cation sites. Among all the phosphates, calcium phosphates $Ca_3(PO_4)_2$ attracts the most attention. For example, tuite γ-$Ca_3(PO_4)_2$ (R-3m and $Z = 3$), the high-pressure polymorph of $Ca_3(PO_4)_2$, any Na-REE systematics could indicate an inconsequential contribution of Si-involving REE exchange mechanism with the melts in the mantle because Si is incompatible with tuite (Konzett and Frost 2009). Whitlockite β-$Ca_3(PO_4)_2$ ($R3c$ and $Z = 21$) is the stable polymorph of $Ca_3(PO_4)_2$ in the shallower horizons of the Earth. Its concentration in REE is widely used to explore the magmatic source region (Sugiyama and Tokonami 1987). Besides, whitlockite is also a common accessory mineral in terrestrial rocks as well as in meteorites from the Mars and the Moon. Many researches have been conducted on the presence and state of whitlockite to explore the terrestrial environment. For example, Hofmann et al. (2006) made a speculation that the upper mantle of Siberia portion should be low in water on the basis of the presence of "anhydrous" whitlockite together with the breakdown of "hydrous" minerals in the xenolith samples from Siberia. In addition to whitlockite, sarcopside ($Fe_{0.8}$, $Mn_{0.2})_{\sum 3}(PO_4)_2$, farringtonite ($Fe_{0.2\sim0.11}$,$Mg_{0.8\sim0.89})_{\sum 3}(PO_4)_2$ and chopinite $(Mg,Fe)_3(PO_4)_2$ are also accessory minerals occasionally in combination in meteorites. It has been documented that they are all formed as a result of high P concentrations in the melts (Grew et al. 2007, 2010). Grew et al. (2010) determined the presence of Mg-enriched sarcopside and the absence of farringtonite in lodranite GRA95209, grounded on which they deduced that the formation of lodranite GRA95209 had suffered an oxidation of P-rich melts, then a Fe–Mg exchange with a large reservoir of Mg-rich silicates and finally a cooling process.

Thus far, investigations on the high-pressure properties of carbonates and phosphates have been conducted comprehensively and intensively, but few literatures on the geochemical behaviors of $[CO_3]^{2-}$ and $[PO_4]^{3-}$ coexistent phases are available now. Such minerals do naturally exist, e.g. carbonate-apatite $Ca_5[PO_4,CO_3(OH)]_3(F,OH)$ and apatite $Ca_5[PO_4]_3(F,Cl,H)$, which can incorporate $[CO_3]^{2-}$ units in the additional anion sites (A site) or the $[PO_4]^{3-}$ sites (B site) (Tacker 2008; Yi et al. 2013). These minerals containing both $[CO_3]$ and $[PO_4]$ groups should possess dual properties of carbonates and phosphates. And the typical samples of such minerals are carbonophosphates, which were discovered in drill cores in Kovdor, Russia, being named as bonshtedtite with the chemical formula of $Na_{3.00}(Fe_{0.63}Mg_{0.17}Mn_{0.06}Na_{0.12})(CO_3)_{1.00}(PO_4)_{1.01}$ and $(Na_{2.99},K_{0.02})(Fe_{0.66}Mg_{0.28}Mn_{0.01})(CO_3)_{0.91}(PO_4)_{1.03}$ (Dunn et al. 1983). Recently, these carbonophosphate minerals have been synthesized in the lab (Chen et al. 2012; Huang et al. 2014). Here, we would like to report a study on the high-pressure behavior of carbonophosphate bradleyite $Na_3Mg(CO_3)(PO_4)$. Bradleyite ($P2_1/m$ and $Z = 2$) is structurally described as a double-layered framework constituted by $[MgO_6]$ octahedra-$[PO_4]^{3-}$ tetrahedra chains along the *b-axis*, where Na atoms occupy two sets of sites: NaI in the fourfold position edge-shared with seven O atoms to form "$[NaIO_7]$–$[NaIO_7]$" chains and NaII in the twofold position to form isolated $[NaIIO_6]$ polyhedra. The coplanar $[CO_3]^{2-}$ units and the isolated

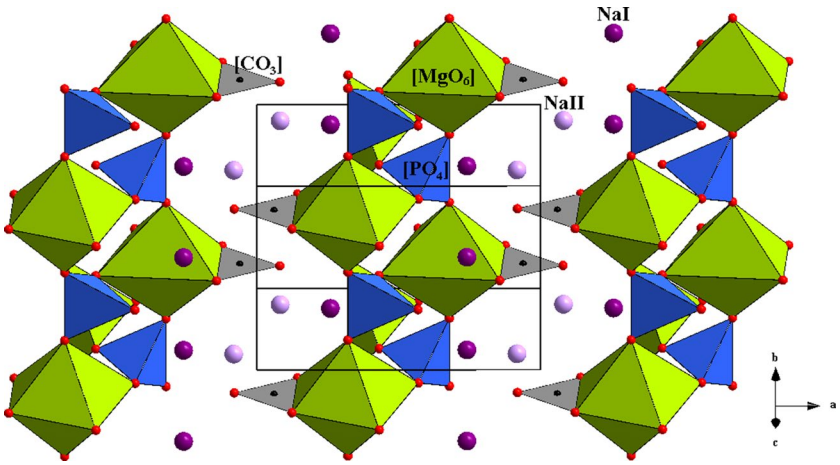

Fig. 1 Crystal structure of bradleyite with the unit-cell outlined. [MgO_6] octahedra are *colored* in *lime*, [PO_4] tetrahedra are *light blue* and [CO_3] *triangles* are *gray*. Na atoms occupy two kinds of sites: NaI coordinates with seven O atoms to form [$NaIO_7$]–[$NaIO_7$] chains, and NaII has six O atom neighbors to form isolated [$NaIIO_6$] polyhedra

[$NaIIO_6$] polyhedra situate the vacant channels to bridge the [MgO_6]–[PO_4] chains and the [$NaIO_7$]–[$NaIO_7$] chains (Fig. 1). The following study will focus on the structural characteristics and the compression mechanism of bradleyite, especially the comparabilities with carbonates and phosphates. The results will provide available information on the geochemical behaviors of bradleyite and throw light upon other carbonophosphates.

Sample and experimental methods

The bradleyite $Na_3Mg(CO_3)(PO_4)$ sample used in the present study was synthesized with excellent purity through a modified hydrothermal solutions. First, 4 mmol $MgSO_4{\cdot}7H_2O$ was dissolved in 10 ml water/ethylene glycol (EG) mixed solution (volume ratio: H_2O/EG = 3:1) to form a clear solution A. Separately, 4 mmol $(NH_4)_2HPO_4$ and 4 g Na_2CO_3 were dissolved in 20 ml H_2O/EG mixed solution (volume ratio: H_2O/EG = 3:1) to form a clear solution B. Solution A was then added to solution B after vigorous stirring, and the mixture slurry was stirred for half an hour. Then, the mixture products were transferred into a 40 ml stainless steel autoclave and heated at 180 °C for 70 h. Later, the products were washed by distilled water five times, followed by drying in a vacuum oven at 80 °C overnight. The synthesized product was characterized at ambient conditions using X-ray diffraction (XRD) and Raman spectroscopy. The diffraction pattern clearly demonstrates that it is a single bradleyite phase ($P2_1/m$ and $Z = 2$). The refined lattice constants are $a = 8.7827(6)$ Å, $b = 6.5970(2)$ Å, $c = 5.1423(2)$ Å and $\beta = 89.621(6)°$, in good agreement with $a = 8.83$ Å, $b = 6.62$ Å, $c = 5.16$ Å and $\beta = 89.69°$ given by Chen et al. (2012).

Pressure was generated using a symmetric-type diamond anvil cell (DAC) with 300 um-diameter anvil culets. The sample chamber was prepared from rhenium gasket with a pre-indented thickness of ~35 μm, and then, drilling a 120 μm-diameter hole in the center of the indented region. The sample was loaded on the surface of an anvil together with a ruby sphere for pressure calibration according to the R1 fluorescence peak position (Mao et al. 1986). To retain a quasi-hydrostatic stress environment, we used neon as the pressure transmitting medium. Reported pressure uncertainties are the differences between the pressure measurements performed before and after each data collection.

High-pressure experiments were performed at 16-ID-B beamline of the HPCAT sector of the Advanced Photon Source (APS), Argonne National Laboratory. A focused monochromatic beam (10 × 10 μm^2) was used with the wavelength of 0.406626 Å. With pressure increasing, twenty-six XRD patterns were reordered using a CCD detector, and the collection time of each pattern was 40 s.

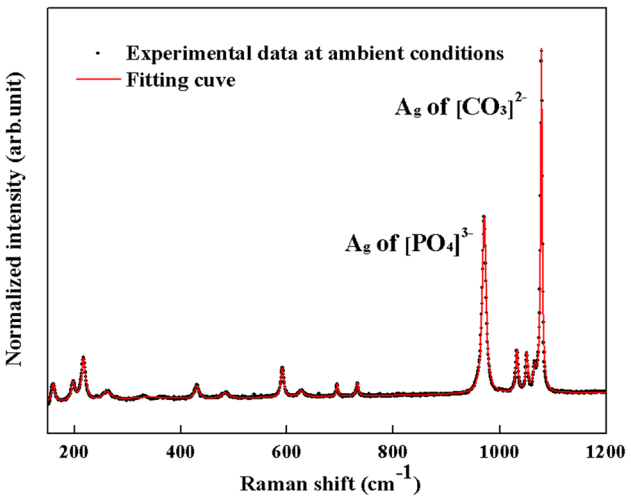

Fig. 2 Raman spectrum of bradleyite at ambient conditions in the range 150–1,200 cm^{-1}. Fifteen Raman bands can be observed, where two strongest peaks (970.8 and 1,078.7 cm^{-1}) are assigned to the symmetrical stretching vibration, respectively, of $[PO_4]^{3-}$ and $[CO_3]^{2-}$ groups

Table 1 Lattice parameters and volume of bradleyite as a function of pressure at room temperature

P (GPa)	*A* (Å)	*B* (Å)	*c* (Å)	*β* (°)	*V* (Å^3)
Compression					
1.9(1)	8.743(1)	6.557(1)	5.119(2)	89.31(1)	293.5(3)
3.0(1)	8.702(2)	6.526(2)	5.093(1)	89.26(1)	289.2(4)
4.1(2)	8.669(1)	6.483(3)	5.056(3)	89.27(2)	284.1(3)
4.9(1)	8.638(2)	6.451(1)	5.041(2)	88.88(1)	280.9(4)
5.8(1)	8.609(1)	6.430(2)	5.020(2)	88.24(1)	277.9(3)
7.0(1)	8.579(1)	6.406(1)	4.996(3)	89.08(2)	274.5(6)
7.8(2)	8.552(1)	6.381(2)	4.967(1)	89.12(1)	271.0(6)
8.9(2)	8.521(1)	6.349(3)	4.941(1)	88.98(1)	267.3(4)
10.5(2)	8.469(3)	6.316(1)	4.922(2)	89.10(1)	263.3(3)
11.8(2)	8.435(2)	6.289(2)	4.896(1)	88.99(2)	259.7(3)
13.2(2)	8.397(2)	6.264(3)	4.875(1)	88.48(1)	256.3(3)
14.6(2)	8.359(1)	6.244(3)	4.843(2)	88.81(3)	252.7(6)
15.6(2)	8.329(3)	6.230(2)	4.827(2)	88.70(2)	250.5(2)
16.8(2)	8.282(3)	6.212(3)	4.804(3)	88.67(1)	247.1(2)
18.1(2)	8.246(2)	6.190(1)	4.784(3)	88.60(2)	244.1(3)
19.7(1)	8.203(1)	6.160(2)	4.754(2)	88.23(1)	240.2(3)
21.9(1)	8.141(3)	6.140(1)	4.707(2)	88.16(2)	235.2(3)
24.3(3)	8.067(2)	6.103(1)	4.683(3)	88.19(3)	230.5(3)
26.2(2)	8.019(2)	6.081(1)	4.652(2)	87.72(2)	226.7(2)
28.4(2)	7.963(3)	6.060(1)	4.628(1)	87.81(1)	223.2(6)
29.8(2)	7.918(3)	6.043(2)	4.609(1)	87.82(1)	220.4(4)
32.0(1)	7.858(1)	6.015(3)	4.583(3)	87.52(2)	216.4(6)
34.4(2)	7.798(1)	6.004(2)	4.550(2)	87.81(3)	212.9(3)
36.4(1)	7.743(2)	5.976(2)	4.513(2)	87.35(3)	208.6(6)
38.4(2)	7.690(2)	5.969(2)	4.495(1)	87.46(2)	206.1(4)
40.9(3)	7.628(3)	5.950(1)	4.475(1)	87.36(1)	202.9(4)
Decompression					
28.4(2)	7.969(3)	6.065(1)	4.632(2)	87.17(2)	223.6(4)
18.4(2)	8.247(2)	6.194(2)	4.781(1)	87.65(2)	244.0(2)
9.1(5)	8.522(3)	6.336(3)	4.934(1)	88.33(3)	266.3(4)
0.0001	8.759(1)	6.599(1)	5.140(1)	89.46(1)	297.1(3)

The number in the parentheses represents one standard deviation in the right-most digit

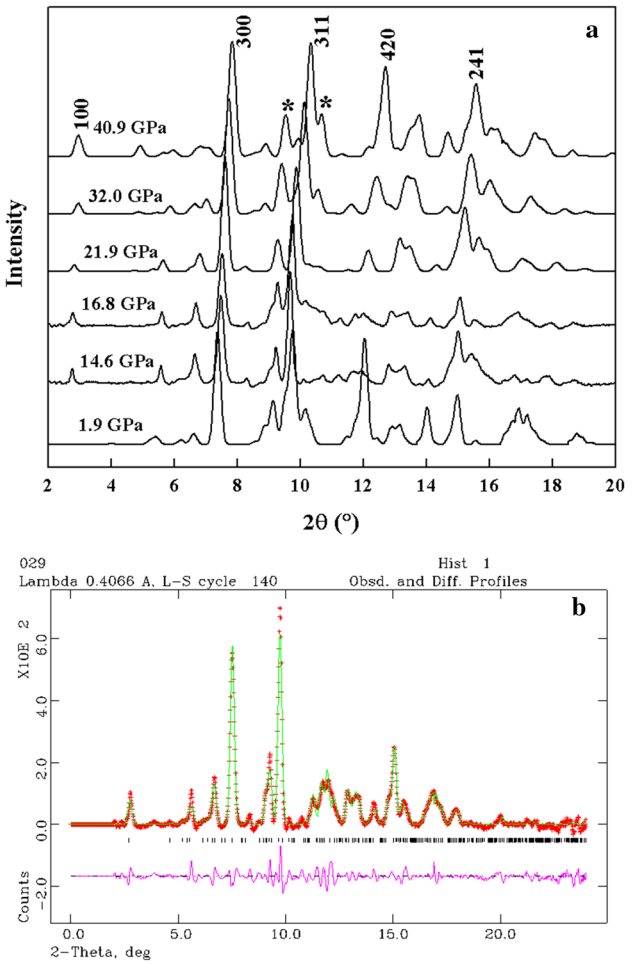

Fig. 3 **a** Representative XRD patterns of bradleyite at various pressures with the background subtracted. The typical peaks are labeled by lattice plane symbol. *Star symbols* represent the diffraction peaks including those from cubic Ne. No discontinuous change close to ~16 GPa can be identified in the patterns. **b** The fitting pattern of 16.8 GPa

Geometry parameters for the radial integration of the two-dimensional data and the sample-to-detector distance (360.5703 mm) were determined from a CeO_2 sample (Jephcoat et al. 1992), and the transformation into standard one-dimensional powder patterns was carried out using the FIT2D software (Hammersley et al. 1996). The one-dimensional diffraction patterns were treated with the general structure analysis system (GSAS) software package using the LeBail method to identify the phase and refine lattice parameters (Larson and Von Dreele 1994).

In Raman spectroscopy experiments conducted at Mineral Physics Laboratory, a Coherent Verdi V2 laser with a 532 nm wavelength was employed for excitation with the power of 400 mW. The spectra were calibrated using the silicon wafer and taken in (unpolarized) backscattering geometry up to 40.6 GPa at room temperature. The collection time for each spectrum was 120 s. All the positions of Raman peaks were fitted using the Peakfit software. At ambient conditions, Raman spectrum shows fifteen peaks in the range 150–1,200 cm^{-1} (Fig. 2), where two strongest symmetrically stretching vibration (A_g) peaks (970.8 and 1,078.7 cm^{-1}) are, respectively, assigned to the $[PO_4]^{3-}$ and $[CO_3]^{2-}$ groups according to the results in previous reports (Gillet et al. 1993; Williams et al. 1993; Santillán and Williams 2004; Zhai et al. 2010). At high pressure, most Raman peaks become obscure due to the strong background from diamond anvils. The following Raman analysis primarily focuses on the evolution of the $[PO_4]^{3-}$ and $[CO_3]^{2-}$ principle stretching vibration modes.

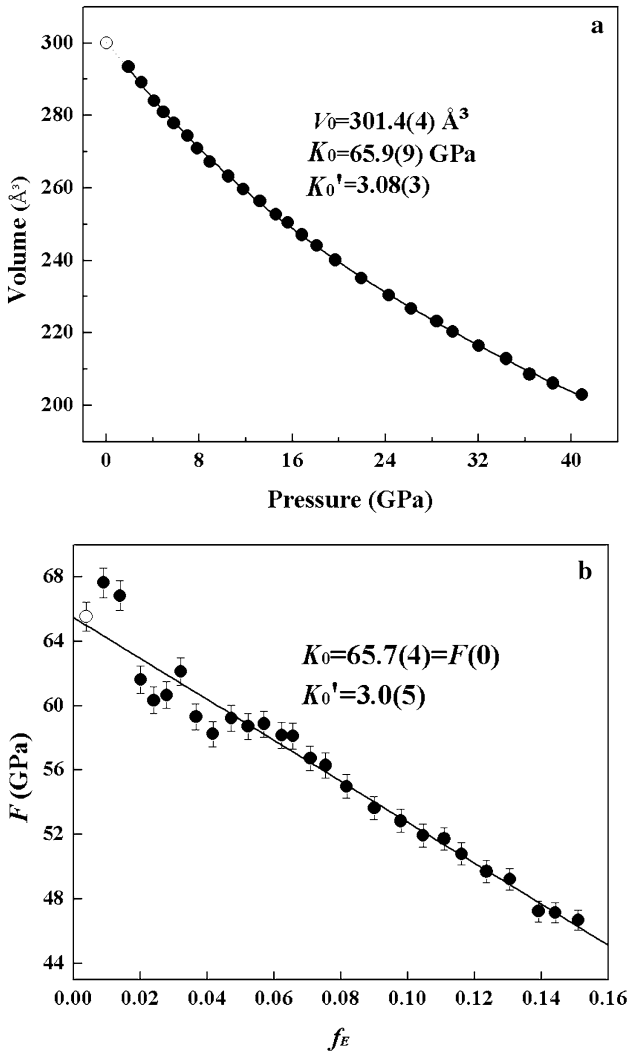

Fig. 4 **a** Pressure–Volume data of bradleyite fitted to the third-order BM EoS. **b** F-f_E plot according to the BM model for bradleyite with K_0, K_0' values listed. The datum expressed by an *open circle* was got at ambient conditions while the high-pressure data were obtained at HPCAT

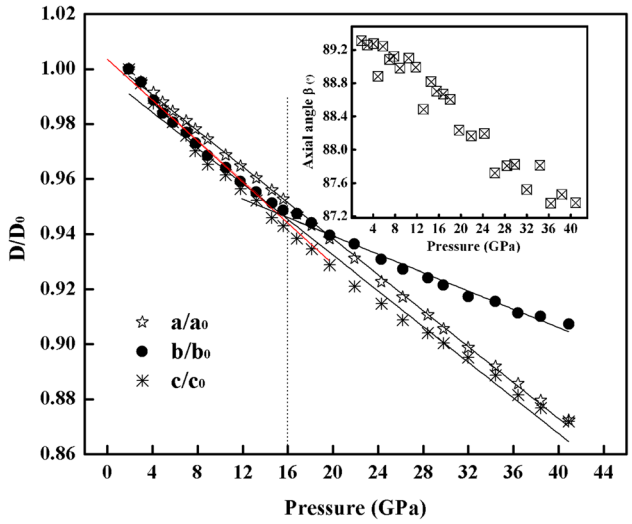

Fig. 5 Normalized axial compression of bradleyite up to 40.9 GPa. The *inset* describes the monotonic decreasing trend of β angle with pressure

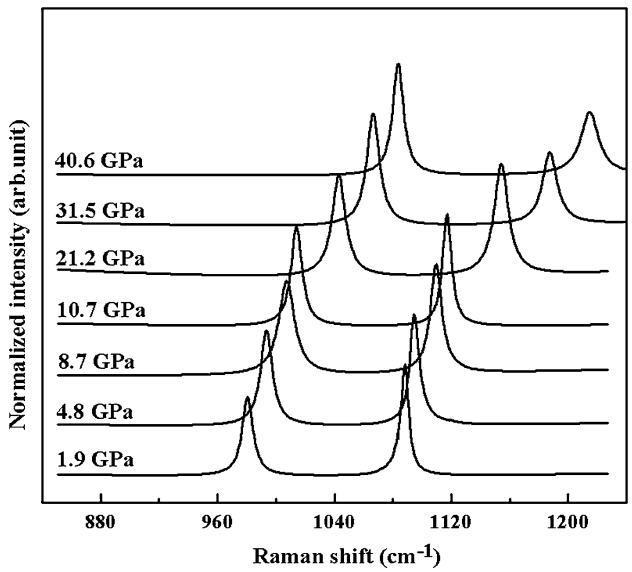

Fig. 6 Representative Raman spectra of bradleyite up to 40.6 GPa. Both symmetrical stretching modes of $[PO_4]^{3-}$ and $[CO_3]^{2-}$ groups shift monotonically and continuously to higher frequencies with pressure

Results

High-pressure XRD data for bradleyite were recorded at room temperature up to 40.9 GPa (Tables 1), and several selected patterns are plotted in Fig. 3a. With pressure increasing, all XRD peaks continuously shift to higher angles and become slightly broader, but no peaks merge or disappear mutationally, indicating that bradleyite is stable in the present pressure conditions. Isothermal pressure–volume data of bradleyite have been fitted to the third-order Birch–Murnaghan equation of state (BM EoS) (Birch 1947) (Fig. 4a), with the least-squares fitting yields values of $K_0 = 65.9(9)$ GPa, $K_0' = 3.08(3)$ and $V_0 = 301.4(4)$ Å^3. To evaluate the quality of BM EoS for the sample studied, the Eulerian strain ($f_E = 1/2[(V_0/V)^{2/3} - 1]$) as a function of the normalized pressure ($F = P/[3f_E(2f_E + 1)5/2]$) is plotted in Fig. 4b (Angel 2000). The inclined slope shows that the first bulk modulus derivative K_0' is smaller than 4, that is, $K_0 = 65.7(4)$ GPa, $K_0' = 3.0(5)$: The intercept corresponds to the bulk modulus, whereas the slope of the straight line provides the first pressure derivative (the slope is equal to $3K_0(K_0' - 4)/2)$, in agreement with our pressure–volume data-fitting results detailed above.

Table 2 Raman frequencies and FWHH of bradleyite on compression

Pressure (GPa)	The $[PO_4]$ groups		The $[CO_3]$ groups	
	Frequency (cm^{-1})	FWHH (cm^{-1})	Frequency (cm^{-1})	FWHH (cm^{-1})
0.2	974.9	9.6	1,078.3	4.8
1.9	982.9	9.0	1,084.0	5.9
2.7	985.9	9.3	1,088.1	5.3
3.7	989.7	9.7	1,090.6	5.9
4.8	993.6	9.9	1,094.5	7.0
6.1	998.7	10.4	1,099.6	7.8
7.4	1,002.8	9.4	1,104.7	7.9
8.7	1,007.4	9.9	1,109.8	7.6
9.6	1,010.7	9.1	1,112.3	7.2
10.7	1,014.6	9.0	1,116.9	7.4
12.1	1,018.6	10.5	1,122.7	8.8
13.4	1,022.5	9.6	1,126.5	9.2
14.5	1,025.6	10.5	1,131.1	9.0
15.4	1,028.3	9.3	1,134.9	9.4
16.4	1,031.0	9.8	1,136.2	10
17.6	1,034.0	9.5	1,140.6	10.1
20.1	1,037.0	10.5	1,145.4	11.6
21.2	1,040.5	10.2	1,151.4	11.8
22.7	1,043.1	10.3	1,153.3	11.1
23.5	1,046.8	10.2	1,160.4	11.4
24.6	1,049.1	10.3	1,161.3	11.7
26.0	1,051.6	10.0	1,164.9	11.3
27.5	1,054.6	9.5	1,170.5	12.1
28.9	1,058.4	9.3	1,174.3	12.6
31.5	1,061.6	10.4	1,178.7	12.1
32.4	1,063.7	9.6	1,181.8	13.0
34.4	1,067.2	10.0	1,187.8	14.7
35.9	1,069.4	9.4	1,190.8	14.0
37.5	1,073.6	9.4	1,197.8	13.4
38.8	1,077.3	9.8	1,201.6	13.8
40.6	1,080.4	9.1	1,207.7	14.7

FWHH full width at half height

In order to acquire the hydrostatic constrains effects on the lattice parameters, we plotted the normalized axial compression, a/a_0, b/b_0 and c/c_0, in Fig. 5. The crystallographic axes exhibit close and considerable compression up to ~16 GPa, but the *b-axis* becomes more and more rigid and results in an increasing anisotropy thereafter. Linear regression analyses $R = R_0 + \gamma \times P$ were applied to fit the axial compression, where R_0 is the value of the refined lattice constants at 0 GPa, γ is the linear compressional coefficient, and P is the pressure. The fitted results are $\gamma_a = -3.27(1) \times 10^{-3}$ GPa^{-1} and $\gamma_c = -3.24(7) \times 10^{-3}$ GPa^{-1}, respectively. For *b-axis* below ~16 GPa, the pressure coefficient is $-3.69(9) \times 10^{-3}$ GPa^{-1}, and at higher pressures it decreases to be $-1.66(6) \times 10^{-3}$ GPa^{-1}. Besides, the evolution of β angle plotted in the insert of Fig. 5 shows a monotonic decreasing trend on compression.

We report variable-pressure Raman spectra in Fig. 6, in which all the symmetrical stretching modes of $[PO_4]^{3-}$ and $[CO_3]^{2-}$ groups shift monotonically and continuously to higher frequencies with pressure (Table 2). Mode band of $[CO_3]^{2-}$ units shifts linearly with a rate of $3.18(2) \times 10^{-3}$ cm^{-1}/GPa; however, the corresponding band associated with $[PO_4]^{3-}$ groups exhibits mode hardening (Fig. 7a). A positive linear slope of $3.54(6) \times 10^{-3}$ cm^{-1}/GPa is observed below ~16 GPa; thereafter, the peak position shifts slowly with pressure coefficient of $2.37(1) \times 10^{-3}$ cm^{-1}/GPa. In simple vibrator model, vibrational frequency is proportional to the square root of force constant. So the observed mode hardening

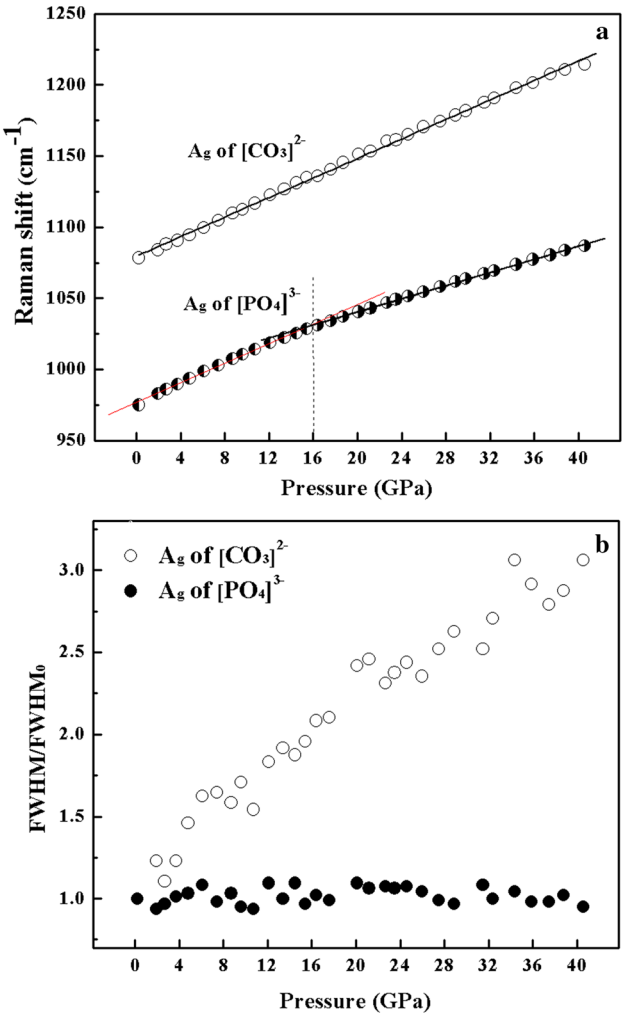

Fig. 7 **a** Pressure-induced Raman shifts of symmetrical stretching vibrations of $[PO_4]^{3-}$ and $[CO_3]^{2-}$ groups in bradleyite. Mode band of $[CO_3]^{2-}$ units shifts linearly, but of $[PO_4]^{3-}$ groups exhibits a mode hardening at ~16 GPa. **b** The pressure-dependent evolution of normalized FWHM of $[PO_4]^{3-}$ and $[CO_3]^{2-}$ groups. Raman band associated with $[PO_4]^{3-}$ groups is invariably narrow up to 40.6 GPa, while of $[CO_3]^{2-}$ units is broadening

means that force constant is more gently strengthening above ~16 GPa, suggestive of the occurrence of some subtle change, which cannot be reflected in the volume reduction but in Raman frequency. In light of pressure coefficients, mode Grüneisen parameters (γ) are readily obtained through $\gamma_i = (\delta\omega_i/\delta P)K_0/\omega_i$, where ω_i is the wavenumber of the ith mode and K_0 is the bulk modulus. We used the obtained isothermal bulk modulus K_0 of 65.9(9) GPa. The calculated γ value is ~0.22 for $[CO_3]^{2-}$ units, ~0.24 for $[PO_4]^{3-}$ groups below ~16 GPa and ~0.16 at higher pressures.

In addition, full width at half maximum (FWHM) of vibrational modes are also analyzed in the present study (Fig. 7b). Over the investigated pressure range, the FWHM of the symmetrical stretching mode of $[PO_4]^{3-}$ groups is invariably narrow and its shape is always sharp, which is attributed to the stable P–O tetrahedral structure and the high degree of order in bradleyite. In contrast, for $[CO_3]^{2-}$ units, the corresponding Raman band is relatively narrow at ambient pressure, but would become broadening on compression. In bradleyite structure, the $[CO_3]^{2-}$ unit shares an edge with $[MgO_6]$ octahedron, and then, the FWHM increases could imply a growing anisotropic behavior between shared and unshared C–O bonds with pressure.

Discussions

Structural characteristics

As described above, bradleyite has a complicated composition containing both $[PO_4]$ and $[CO_3]$ groups. The $[PO_4]$ tetrahedra in the bradleyite structure play an architectural role combined with $[MgO_6]$ octahedra to form the double-layered framework of $[MgO_6]$–$[PO_4]$–$[MgO_6]$–$[PO_4]$ along the *b-axis*, whereas the $[CO_3]$ triangles sit in the vacant channels linking different polyhedral sheets. Na occupy two kinds of large site with the mean interatomic distance Na–O being ~2.5 Å. This general construction of carbonophosphate is scarce in most phosphates, such as magnesium phosphate $Mg_3(PO_4)_2$, zinc phosphate $Zn_3(PO_4)_2$ and manganese phosphate $Mn_3(PO_4)_2$, but exhibits somewhat similarities to tricalcium phosphate $Ca_3(PO_4)_2$. Here, we give interpretations using $Mg_3(PO_4)_2$ and $Ca_3(PO_4)_2$ as structural models. In $Mg_3(PO_4)_2$, there exists two types of Mg sites: MgI has five O atom neighbors belonging to four different $[PO_4]$ tetrahedra, and MgII coordinates with O atoms of six different $[PO_4]$ tetrahedra. However, no distinctive polyhedral chains can be distinguished, and the length of Mg–O bond is shorter at ~2.0 Å (Nord and Kierkrgaare 1968). For compound $Ca_3(PO_4)_2$, two polymorphs should be noted, one is the β-phase (whitlockite) that existed at ambient conditions, and the other is the γ-phase (tuite) that is stable at higher pressure. Both phases are characterized with distinct polyhedral sequences. The whitlockite phase has two types of chains along the *c-axis*, one is $[PO_4]$–$[CaIO_8]$–$[CaIIIO_8]$–$[CaIIO_8]$–$[PO_4]$, and the other is $[PO_4]$–$[CaIVO_9]$(50 %)–□–$[CaVO_6]$–□, in which □ represents the structural vacancy. The tuite structure is featured with one type of interconnected polyhedral sequence of $[PO_4]$–$[CaIIO_{10}]$–$[CaIO_{12}]$–$[CaIIO_{10}]$–$[PO_4]$ along the *c-axis*. Both whitlockite and tuite contain larger Ca^{2+} sites and longer Ca–O bonds (~2.6 Å) (Nord and Kierkrgaare 1968; Zhai et al. 2009).

Different from the $[PO_4]$ group, the $[CO_3]$ unit in bradleyite is just like interstitial ions. Indeed in phosphates, when larger $[PO_4]$ tetrahedra bond is with small divalent cation

(e.g. Mg^{2+}, Zn^{2+}, Fe^{2+}, Mn^{2+}, and even Ca^{2+}), the divalent cation tends to be wrapped around by a layer of hydrone (H_2O) to form hydration cation to offset the size differences and maintain stability. The [CO_3] unit in bradleyite is just as the hydrone in phosphates. And this may be the reason of structural stability of bradleyite up to 41 GPa, whereas phosphates would easily transform to denser phases at higher pressures (Annersten and Nord 1980). The local placement of [CO_3] units in bradleyite is distinctively different from those in carbonates, where the [CO_3] triangles are framesets sharing three O atoms with the neighbor [MO_6] (M = Ca, Mg, Zn, Fe, etc.) octahedra; however, in bradleyite, the [CO_3] triangles act as bridges edge-linked to [MgO_6] octahedra and [$NaIO_6$] polyhedra. Overall, the total composition can be roughly deemed as $NaMg(PO_4) + Na_2CO_3$.

Irrespective of structural distinctiveness from phosphates and carbonates, the bradleyite phase would possibly evolve from apatite, or rather fluorapatite $Ca_5(PO_4)_3F$ structure (Klemme and Dalpé 2003). The apatite structure can be schematized with CaI and CaII polyhedra forming columns around the *c-axis* and being connected by the isolated [PO_4] tetrahedra. F, Cl and OH are disposed in columns on the sixfold screw axes. This kind of structure allows a certain amount of substitution of $[CO_3]^{2-}$ for $[PO_4]^{3-}$ and Na^+ for Ca^{2+}, generally adjusting the types and proportions of additional anions to maintain neutral. The transition from apatite (fluorapatite) phase to bradleyite framework has been proposed to be realized because the transformation between hexagonal and monoclinic based on substitution has been evidenced in calcium phosphate minerals, with the atomic positions being similar in two symmetries (Hughes et al. 1990; Mackie and Young 1974).

Compressional mechanisms

The bulk modulus of bradleyite obtained here is $K_0 = 65.9(9)$ GPa with $K_0' = 3.08(3)$ and $V_0 = 301.4(4)$ Å^3. The value of $K_0 = 65.9(9)$ GPa is obviously smaller comparing with that of tuite γ-$Ca_3(PO_4)_2$, which has the K_0 value of 100.2(13) GPa with $K_0' = 5.48(16)$, and 113.1(12) GPa with $K_0' = 4$(fixed) (Zhai et al. 2009). The fact that the bulk modulus of bradleyite is smaller than that of tuite can be readily understood through the structure characteristics. In bradleyite, there exist periodically arranged channels to be the direct resistance to the external pressure and exhibit high compressibility when the crystal volume is under reduction. However, in tuite, all the [PO_4]–[$CaIIO_{10}$]–[$CaIO_{12}$]–[$CaIIO_{10}$]–[PO_4] polyhedral sequences are interconnected without obvious interspace. Based on the conclusion that the [PO_4] tetrahedron are about three times more incompressible compared to Ca polyhedra (Comodi et al. 2001b), the volume compression of tuite is principally produced from the contraction in Ca polyhedra, which are relatively incompressible than the vacant channels in bradleyite. In fact, many minerals containing channels have lower K_0 values. For example, fluorapatite contains channel to represent the most compressible direction (//[001]) and its bulk modulus is 93(4) GPa with $K_0' = 5.8(1.8)$, smaller than that of tuite. Heulandite has more compressible channels exhibiting softer behavior with $K_0 = 15(8)$ GPa (Gillet et al. 1996). Besides, the K_0 value of bradleyite is also generally smaller than that of carbonates containing divalent cations with similar radii. Fitting to the BM EoS with $K_0' = 4$(fixed), the K_0 value is 137(3) GPa, 126.8(6) GPa and 126(10) GPa for magnesite $MgCO_3$, smithsonite $ZnCO_3$ and rhodochrosite $MnCO_3$ (Fiquet et al. 1994; Ono 2007; Gao et al. 2014), respectively. In conclusion, carbonophosphates (bradleyite) are more compressible phases relative to phosphates and carbonates, which is mainly due to the existence of vacant channels to yield much volume contraction.

Based on the fact that the bradleyite structure can be transformed from that of apatite (fluorapatite), it is reasonable to find that the bulk modulus of bradleyite is close to that of carbonated apatite. Bradleyite with a high content of [CO_3] (22 wt%) as the interstitial ions was determined here to have a lower value of $K_0 = 65.9(9)$ GPa with $K_0' = 3.08(3)$. Liu et al. (2011) investigated the EoS of carbonated hydroxylapatite samples and found that the sample whose channel $[OH]^-$ was almost completely replaced by the [CO_3] units (~80 % 11.2 wt% [CO_3]) (type A) has the K_0 value of 73(2) GPa and $K_0' = 7.0(6)$. And the sample with type B [CO_3] groups (4.8 wt %) has a larger K_0 value of 89(2) GPa with $K_0' = 4.1(6)$. Besides, the pure fluorapatite exhibits a much larger $K_0 = 93(4)$ GPa, $K_0' = 5.8(1.8)$ (Comodi et al. 2001a, b). All the results are suggestive that the accommodation of [CO_3] units in the apatite structure would significantly reduce the bulk modulus; in other words, the stability of apatite would decrease in the presence of [CO_3] or carbonates.

Bradleyite structure does not have a strong compressional anisotropy below ~16 GPa, and the crystallographic axes exhibit close compressional coefficients of 3.2–3.5 $\times$ 10^{-3}. The low anisotropy has already been discovered in tuite (Zhai et al. 2009), fluorapatite (Comodi et al. 2001b), apatite (Matsukage et al. 2004) and carbonated hydroxylapatite (Liu et al. 2011). The most obvious distinction of bradleyite is the change in relative axial compressibility: In spite of the considerable compression of crystallographic axes below ~16 GPa, a growing anisotropy (γ_b/γ_a and γ_b/γ_c) can be identified at higher pressures. The variation in relative axial compressibility is bound to change the relative axial lengths and then even change the whole symmetry. This phenomenon is scarce in simple carbonates or phosphates. Indeed in carbonates, the *c-axis* is generally

about three times more compressible than the *a-axis* (Liu and Lin 1997; Ono 2007; Minch et al. 2010; Gao et al. 2014). And in tuite γ-$Ca_3(PO_4)_2$, the axial compressibilities along *a-axis* and *c-axis* are equal to 2.87 × 10^{-3} and 2.12 × 10^{-3} Å GPa^{-1} up to 40.29 GPa, respectively, derived from the experimental data of Zhai et al. (2009). However, in carbonated hydroxylapatite, the elastic anisotropy is reducing on compression (Liu et al. 2011).

Behaviors of $[PO_4]^{3-}$ and $[CO_3]^{2-}$ groups in bradleyite, carbonates or phosphates

Raman spectroscopy is a useful technique to probe into the characteristics of anion groups. Most reports have demonstrated that the Raman modes of $[PO_4]^{3-}$ and $[CO_3]^{2-}$ groups, respectively, in phosphates or carbonates would shift to higher frequencies with pressure, and this is also observed in bradleyite. The pressure dependence of $[PO_4]^{3-}$ mode shifts in bradleyite is calculated to be ~3.54(6) × 10^{-3} cm^{-1}/GPa below ~16 GPa, which is a little lower than 4.1 × 10^{-3} in tuite γ-$Ca_3(PO_4)_2$ (Zhai et al. 2010), and 4.8 × 10^{-3} in fluorapatite $Ca_5(PO_4)_3F$ (Comodi et al. 2001a). The symmetrical stretching vibration is structurally related to the P–O bond compressibility; therefore, the lower value indicates that the P–O bond in bradleyite is more incompressible than that in tuite/fluorapatitie. The difference in P–O bond compressibility in bradleyite and phosphates corresponds well with the work of Comodi et al. (2001b). Comodi et al. (2001b) investigated the $[PO_4]$ evolution in several minerals and discovered that when the $[PO_4]$ tetrahedra arrange orderly with other polyhedra (e.g. berlinite $AlPO_4$), the $[PO_4]$ tetrahedra do not change with pressure; however, when the $[PO_4]$ tetrahedra are isolated arrangement (e.g. apatite), the bulk modulus can be measured as 270(10) GPa. Accordingly, for bradleyite containing an ordered distribution of $[PO_4]$ tetrahedra-$[MgO_6]$ octahedra-Na polyhedra, the $[PO_4]$ tetrahedra would remain unchanged on compression, and thus, the P–O bond exhibits more rigid behavior relative to that in tuite or apatite (fluorapatite).

Above ~16 GPa, the P–O bond presents a mode hardening, indicative of the occurrence of some subtle change in the local structure. Williams and Knittle (1996) put forward that the $[PO_4]$ site symmetry would increase under compression, but Comodi et al. (2001a) proposed that rather than the $[PO_4]$ tetrahedra themselves, it was the symmetry of the environment around the $[PO_4]$ tetrahedra that increase because $[PO_4]$ tetrahedra are much more incompressible than Ca polyhedra. Accordingly, in bradleyite with pressure, the $[PO_4]$ tetrahedra would remain unchanged while the Na polyhedra become regular, and the original arrangement of $[PO_4]$–$[MgO_6]$-Na polyhedra changes. The variation of $[PO_4]$–$[MgO_6]$–Na polyhedra distribution has an effect on the local environment of the $[PO_4]$ tetrahedra, thus affecting the $[PO_4]$ evolution, which has been observed as the mode hardening at ~16 GPa in our Raman spectra.

Mode Griineisen parameter (γ) provides a good tool by which the contributions of Raman mode to the dynamic properties of minerals may be evaluated. Here, we obtained the γ values in bradleyite to be ~0.22 for $[CO_3]^{2-}$ units, ~0.24 for $[PO_4]^{3-}$ groups below ~16 GPa and ~0.16 at higher pressures. We also refer to the data from previous reports for intercomparison purposes. Williams et al. (1993) studied the corresponding mode of $[CO_3]^{2-}$ units in magnesite and obtained almost identical γ value of 0.24(2). Santillán and Williams (2004) studied the asymmetric stretching vibration and bending vibrations of $[CO_3]^{2-}$ units in siderite $FeCO_3$ and rhodochrosite $MnCO_3$, and also determined the approximate values (0.1–0.4). The average γ value of the internal modes of $[PO_4]^{3-}$ groups in tuite has been obtained to be 0.36 (Zhai et al. 2010), while in fluorapatite to be 0.44 (Comodi et al. 2001a). These low γ values are compatible with the incompressibility of both anion groups. The incompressibility of $[PO_4]^{3-}$ and $[CO_3]^{2-}$ groups does not contradict the low K_0 value of bradleyite because the evolution of the $[PO_4]^{3-}$ and $[CO_3]^{2-}$ groups are not representative of the structural variation on the whole, yet it appears that the Na polyhedra and the vacant channels strongly affect the bulk modulus.

The discovery of carbonophosphate minerals in the Earth indicates noteworthy significance. Firstly, the existence of bradleyite may open new perspectives on the Earth carbon and phosphorus cycle. Since carbonophosphate minerals have been synthesized successfully through hydrothermal solutions of carbonates with hydrophosphates in the laboratory, there thus exist possibilities that carbonophosphates could be produced from carbonatite fluid contaminated by phosphates during the subduction to the Earth's mantle (Frezzotti et al. 2011). However, during to the low density structures, the carbonophosphate phases are likely to decompose to dense carbonate and phosphate at the mantle conditions; otherwise instead of decomposition, carbonophosphates would first release $[CO_3]^{2-}$ groups into the melts because the $[CO_3]^{2-}$ groups in the structures are just like interstitial ions. The $[CO_3]^{2-}$ fluid in the lower mantle has a significant influence on a number of physical and chemical properties, such as lower the melting point, improve the electrical conductivity, induce the partial melting, and thus, affect the mantle's chemical differentiation and help interpret the observed lower velocity region in the upper mantle (Presnall et al. 2002; Gaillard et al. 2008; Dasgupta and Hirschmann 2010). As for the Earth phosphorus cycle, Joswig et al. (1999) has suggested that a considerable amount of phosphorus can be brought to the mantle via the down-going slab, but its phases in the mantle remain ill defined. Phosphates have long been considered as the main phosphorus-bearing minerals, but their stability

might be somewhat reduced by the incorporation of $[CO_3]$ or carbonates (Liu et al. 2011). Herewith, the first evidence of carbonophosphate bradleyite, which can evolve from the apatite (fluorapatite) phase, we proposed that carbonophosphates should be a potential carrier during the phosphorus transfer, and control its geochemistry in a certain range. From the perspective of the structural relations to some phosphates (e.g. whitlockite, tuite and apatite), carbonophosphates could also exhibit equivalent capacity to incorporate large elements, such as LILE and REE. In addition to the large Na^+ sites, the vacant channels would exhibit a stronger self-regulating capacity to accommodate extraneous elements. Even though bradleyite has been discovered as a trace mineral in the Earth, its geochemical behavior will shed light on other carbonophosphates, as well as other minerals crystallized from carbonate–phosphate systems.

Conclusions

The high-pressure behavior of carbonophosphate bradleyite $Na_3Mg(CO_3)(PO_4)$ was explored through synchrotron radiation XRD combined with Raman spectroscopy at pressures up to ~41 GPa. Bradleyite is a representative of $[CO_3]^{2-}$ and $[PO_4]^{3-}$ coexistent minerals, with a double-layered structure constituted of $[MgO_6]$–$[PO_4]$–$[MgO_6]$–$[PO_4]$ along the *b-axis*, where the $[NaIO_7]$–$[NaIO_7]$ chains sit aside in the vacant channels linked by $[CO_3]$ triangles and $[NaIIO_6]$ polyhedra. This kind of structure is distinctive from that of orthophosphates or carbonates, but has been proposed to be transformed from apatite (fluorapatite) phase. Our study proved its stability in the $P2_1/m$ ($Z = 2$) phase, and the isothermal pressure–volume relationship was described using the third-order BM EoS with $K_0 = 65.9(9)$ GPa, $K_0' = 3.08(3)$ and $V_0 = 301.4(4)$ Å^3. The lower K_0 value implies that bradleyite is more compressible in comparison with carbonates and phosphates, but has similar compressibility to carbonated apatite. Axial compressibilities show considerable condensability, and an increasing anisotropy can be defined thereafter because the *b-axis* becomes more and more rigid. FWHM of Raman band is a measurement of the order degree of structure. Raman band of $[PO_4]^{3-}$ groups is invariably narrow with sharp shape in the investigated pressure range, while of $[CO_3]^{2-}$ units is broadening, which can be accounted for by the anisotropic behavior between shared and unshared C–O bonds with pressure increasing. The rigidness of $[CO_3]^{2-}$ and $[PO_4]^{3-}$ groups in bradleyite are compatible with those, respectively, in carbonates and phosphates. The discovery and the stability of carbonophosphate bradleyite up to 41 GPa at room temperature could bring up new views on the Earth carbon and phosphorus cycle. And the structural similarity to some phosphates suggests the potential capacity of carbonophosphate minerals to be the reservoirs of large trace elements.

Acknowledgments The authors would like to thank Jie Zhu and Jin Liu for their assistances in experiments. This work was supported by Natural Science Foundation of China (Grant No. U1232204). Synchrotron works of the study were performed at HPCAT of the APS, ANL. HPCAT operations are supported by DOE-NNSA under Award No. DE-NA0001974 and DOE-BES under Award No. DE-FG02-99ER45775, with partial instrumentation funding by NSF. APS is supported by DOE-BES, under Contract No. DE-AC02-06CH11357.

References

Angel RJ (2000) Equations of State. In: Hazen RM, Downs RT (eds) Reviews in mineralogy and geochemistry. Mineralogical Society of America, Chantilly, pp 35–39

Annersten H, Nord AG (1980) A high pressure phase of magnesium orthophosphate. Acta Chem Scand Ser A 34:389–390

Biellmann C, Gillet P, Guyot F, Peyronneau J, Reynard B (1993) Experimental evidence for carbonate stability in the Earth's lower mantle. Earth Planet Sci lett 118:31–41

Birch F (1947) Finite elastic strain of cubic crystals. Phys Rev Lett 71:809–924

Boulard E, Menguy N, Auzende AL, Benzerara K, Bureau H, Antonangeli D, Corgne A, Morard G, Siebert J, Perrillat JP, Guyot F, Fiquet G (2012) Experimental investigation of the stability of Fe-rich carbonates in the lower mantle. J Geophys Res 117:B02208

Buob A, Luth RW, Schmidt MW, Ulmer P (2006) Experiments on $CaCO_3$–$MgCO_3$ solid solutions at high pressure and temperature. Am Mineral 91:435–440

Chen HL, Hautier G, Ceder G (2012) Synthesis, computed stability, and crystal structure of a new family of inorganic compounds: carbonophosphates. J Am Chem Soc 134(48):19619–19627

Comodi P, Liu Yu, Frezzotti ML (2001a) Structural and vibrational behaviour of fluorapatite with pressure. Part II: in situ micro-Raman spectroscopic investigation. Phys Chem Miner 28:225–231

Comodi P, Liu Yu, Zanazzi PF, Montagnoli M (2001b) Structural and vibrational behaviour of fluorapatite with pressure Part I: in situ single-crystal X-ray diffraction investigation. Phys Chem Miner 28:219–224

Dasgupta R, Hirschmann MM (2010) The deep carbon cycle and melting in Earth's interior. Earth Planet Sci Lett 298:1–13

Dunn PJ, Grice JD, Fleischer M, Pabst A (1983) New mineral names. Am Mineral 68:1038–1041

Fiquet G, Guyot F, Itie JP (1994) High-pressure X-ray diffraction study of carbonates: $MgCO_3$, $CaMg(CO_3)_2$, and $CaCO_3$. Am Mineral 79:15–23

Franzolin E, Schmidt MW, Poli S (2011) Ternary Ca–Fe–Mg carbonates: subsolidus phase relations at 35 GPa and a thermodynamic solid solution model including order/disorder. Contrib Mineral Petrol 161(2):13–227

Frezzotti ML, Selverstone J, Sharp ZD, Compagnoni R (2011) Carbonate dissolution during subduction revealed by diamond-bearing rocks from the Alps. Nat Geosci 4:703–706

Gaillard F, Malki M, Iacono-Marziano G, Pichavant M, Scaillet B (2008) Carbonatite melts and electrical conductivity in the asthenosphere. Science 322:1363–1365

Gao J, Zhu F, Lai XJ, Huang R, Qin S, Chen DL, Liu J, Zheng LR, Wu X (2014) Compressibility of a natural smithsonite $ZnCO_3$ up to 50 GPa. High Pressure Res 34(1):89–99

Gillet P, Biellmann C, Reynard B, McMillan P (1993) Raman spectroscopic studies of carbonates. Part I: high-pressure and high-temperature behaviour of calcite, magnesite, dolomite and aragonite. Phys Chem Miner 20:1–18

Gillet P, Malezieux JM, Itié JP (1996) Phase changes and amorphization of zeolite at high pressures: the case of scolecite and mesolite. Am Mineral 81:651–657

Goldsmith JR, Graf DL, Witters J, Northrop D (1962) Studies in the system $CaCO_3$–$MgCO_3$–$FeCO_3$:1. Phase relations; 2. A method for the major-element spectrochemical analysis; 3. Composition of some ferroan dolomites. J Geol 70:659–688

Grew ES, Armbruster T, Medenbach O, Yates MG, Carson CJ (2007) Chopinite, [(Mg, Fe)3X](PO4)2, a new mineral isostructural with sarcopside, from a fluorapatite segregation in granulite-facies paragneiss, Larsemann Hills, Prydz Bay, East Antarctica. Eur J Mineral 19:229–245

Grew ES, Yates MG, Beane RJ, Floss C, Gerbi C (2010) Chopinite-sarcopside solid solution, [(Mg, Fe)3X](PO4)2, in GRA95209, a transitional acapulcoite: implications for phosphate genesis in meteorites. Am Mineral 95:260–272

Hammersley AP, Svensson SO, Hanfland M, Fitch AN, Hausermann D (1996) Two-dimensional detector software: from real detector to idealised image or two-theta scan. High Pressure Res 14:235–248

Hofmann AW, Merlet C, Gurenko AA, Hellebrand E, Montagnac G, Gillet P, Prikhodko VS, Ionov DA (2006) Discovery of whitlockite in mantle xenoliths: inferences for water- and halogen-poor fluids and trace element residence in the terrestrial upper mantle. Earth Planet Sci Lett 244:201–277

Huang WF, Zhou J, Li B, Ma J, Tao S, Xia DG, Chu WS, Wu ZY (2014) Detailed investigation of $Na_{2.24}FePO_4CO_3$ as a cathode material for Na-ion batteries. Sci Rep. doi:10.1038/srep04188

Hughes JM, Cameron M, Crowley KD (1990) Crystal structures of natural ternary apatites: solid solution in the Ca5[PO4]3X (X = F, OH, Cl) system. Am Mineral 75:295–304

Jephcoat AP, Finger LW, Cox DE (1992) High pressure, high resolution synchrotron X-ray powder diffraction with a position-sensitive detector. High Pressure Res 8:667–676

Joswig W, Stachel T, Harris JW, Baur WH, Brey GP (1999) New Ca-silicate inclusions in diamonds-tracers from lower mantle. Earth Planet Sci Lett 173:1–6

Klemme S, Dalpé C (2003) Trace-element partitioning between apatite and carbonatite melt. Am Mineral 88:639–646

Konzett J, Frost DJ (2009) The high P-T stability of hydroxyl-apatite in natural and simplified MORB- an experimental study to 15 GPa with implications for transport and storage of phosphorus and halogens in subduction zones. J Petrol 50(11):2043–2062

Larson AC, Von Dreele RB (1994) General structure analysis system (GSAS). Los Alamos Natl Lab 86–748

Lin JF, Liu J, Jacobs C, Prakapenka VB (2012) Vibrational and elastic properties of ferromagnesite across the electronic spin-pairing transition of iron. Am Mineral 97:583–591

Liu LG, Lin CC (1997) A calcite → aragonite-type phase transition in $CdCO_3$. Am Mineral 82:643–646

Liu X, Shieh SR, Flee ME, Zhang L, Qiang H (2011) Equation of state of carbonated hydroxylapatite at ambient temperature up to 10 GPa: significance of carbonate. Am Mineral 96:74–80

Mackie PE, Young RA (1974) Fluorine-chlorine interaction in fluorchlorapatite. J Solid State Chem 11:319–329

Mao HK, Xu J, Bell P (1986) Calibration of the ruby pressure gauge to 800 kbar under quasi-hydrostatic conditions. J Geophys Res 91:4673–4676

Mao Z, Armentrout M, Rainey E, Manning CE, Dera P, Prakapenka VB, Kavner A (2011) Dolomite III: a new candidate lower mantle carbonate. Geophys Res Lett 38:L22303

Martin AM, Hammouda T (2011) Role of iron and reducing conditions on the stability of dolomite + coesite between 4.25 and 6 GPa-A potential mechanism for diamond formation during subduction. Eur J Mineral 123:5–16

Martinez I, Zhang J, Reeder RJ (1996) In situ X-ray diffraction of aragonite and dolomite at high pressure and high temperature: evidence for dolomite breakdown to aragonite and magnesite. Am Mineral 81:611–624

Matsukage KN, Ono S, Kawamoto T, Kikegawa T (2004) The compressibility of a natural apatite. Phys Chem Miner 31(9):580–584

Merlini M, Crichton WA, Hanfland M, Gemmi M, Müller H, Kupenko I, Dubrovinsky L (2012a) Structures of dolomite at ultrahigh pressure and their influence on the deep carbon cycle. PNAS 109:13509–13514

Merlini M, Hanfland M, Crichton WA (2012b) $CaCO_3$-III and $CaCO_3$-VI, high-pressure polymorphs of calcite: possible host structures for carbon in the Earth's mantle. Earth Planet Sci Lett 333–334:265–271

Merrill L, Bassett WA (1975) The crystal structure of $CaCO_3$ (II), a high-pressure metastable phase of calcium carbonate. Acta Crystallogr B 31:343

Minch R, Seoung DH, Ehm L, Winkler B, Knorr K, Peters L, Borkowski LA, Parise JB, Lee Y, Dubrovinsky L, Depmeier W (2010) High pressure behavior of otavite ($CdCO_3$). J Alloy Compd 508:251–257

Nord AG, Kierkrgaare P (1968) The crystal structure of $Mg_3(PO_4)_2$. Acta Chem Scand 22:1466–1474

Oganov AR, Glass CW, Ono S (2006) High-pressure phases of $CaCO_3$: crystal structure prediction and experiment. Earth Planet Sci Lett 241:95–103

Ono S (2007) High-pressure phase transformation in $MnCO_3$: a synchrotron XRD study. Mineral Mag 71(1):105–111

Ono S, Kikegawa T, Ohishi Y, Tsuchiya J (2005) Post-aragonite phase transformation in $CaCO_3$ at 40 GPa. Am Mineral 90:667–671

Presnall DC, Gudfinnsson GH, Walter MJ (2002) Generation of mid-ocean ridge basalts at pressures from 1 to 7 GPa. Geochim Cosmochim Acta 66:2073–2090

Santillán J, Williams Q (2004) A high-pressure infrared and X-ray study of $FeCO_3$ and $MnCO_3$: comparison with $CaMg(CO_3)_2$-dolomite. Phys Earth Planet Inter 143–144:291–304

Shannon RD (1976) Revised effective ionic radii and systematic studies of interatomic distances in halides and chalcogenides. Acta Cryst A32:751–767

Stagno V, Tange Y, Miyajima N, McCammon CA, Irifune T, Frost DJ (2011) The stability of magnesite in the transition zone and the lower mantle as function of oxygen fugacity. Geophysical Res Lett 38:L19309

Sugiyama K, Tokonami M (1987) Structure and crystal chemistry of a dense polymorph of tricalcium phosphate $Ca_3(PO_4)_2$: a host to accommodate large lithophile elements in the Earth's mantle. Phys Chem Miner 15:125–130

Tacker RC (2008) Carbonate in igneous and metamorphic fluorapatite: two type A and two type B substitutions. Am Mineral 93:168–176

Williams Q, Knittle E (1996) Infrared and Raman spectra of $Ca_5(PO_4)_3F$-fluorapatite at high pressure: compression-induced changes in phosphate site and Davydov splittings. J Phys Chem Solid 57(4):417–422

Williams Q, Collerson B, Knittle E (1993) Vibrational spectra of magnesite ($MgCO_3$) and calcite-III at high pressures. Am Mineral 77:1158–1165

Yi HH, Balan E, Gervais C, Segalen L, Fayon F, Roche D (2013) A carbonate-fluoride defect model for carbonate-rich fluorapatite. Am Mineral 98:1066–1069

Zhai SM, Liu X, Shien S, Zhang LF, Ito E (2009) Equation of state of γ-tricalcium phosphate, γ-$Ca_3(PO_4)_2$, to lower mantle pressures. Am Mineral 94:1388–1391

Zhai SM, Wu X, Ito E (2010) High-pressure Raman spectra of tuite, γ-$Ca_3(PO_4)_2$. J Raman Spectrosc 41:1011–1013